# Analysis of WASp function during the wound inflammatory response – live-imaging studies in zebrafish larvae

**Ana Cvejic[1,2], Chris Hall[3], Magdalena Bak-Maier[1], Maria Vega Flores[3], Phil Crosier[3], Michael J. Redd[4] and Paul Martin[1,*]**

[1]Departments of Biochemistry and Physiology, School of Medical Sciences, University of Bristol, Bristol BS8 1TD, UK
[2]Department of Haematology, University of Cambridge, Cambridge CB2 2PT, UK
[3]Department of Molecular Medicine and Pathology, School of Medical Sciences, The University of Auckland, Auckland, New Zealand
[4]Huntsman Cancer Institute, University of Utah, Salt Lake City, UT 84112, USA
*Author for correspondence (e-mail: paul.martin@bristol.ac.uk)

*Accepted 8 July 2008*
*Journal of Cell Science 121, 3196-3206 Published by The Company of Biologists 2008*
*doi:10.1242/jcs.032235*

## Summary

**Wiskott-Aldrich syndrome protein (WASp) is haematopoietically restricted, and is the causative protein underlying a severe human disorder that can lead to death due to immunodeficiency and haemorrhaging. Much is known about the biochemistry of WASp and the migratory capacity of WASp-defective cells in vitro, but in vivo studies of immune-cell behaviour are more challenging. Using the translucency of zebrafish larvae, we live-imaged the effects of morpholino knockdown of WASp1 (also known as Was) on leukocyte migration in response to a wound. In embryos at 22 hours post-fertilisation, primitive macrophages were impaired in their migration towards laser wounds. Once a circulatory system had developed, at 3 days post-fertilisation, we observed significantly reduced recruitment of neutrophils and macrophages to ventral fin wounds. Cell-tracking studies indicated that fewer leukocytes leave the vessels adjacent to a wound and those that do exhibit impaired navigational capacity. Their cell morphology appears unaltered but their choice of leading-edge pseudopodia is more frequently incorrect, leading to impaired chemotaxis. We also identified two zebrafish mutants in WASp1 by TILLING, one of which was in the WIP-binding domain that is the hotspot for human lesions, and mutants exhibited the same deficiencies in wound inflammation and thrombus formation as WASp1 morphants.**

Supplementary material available online at
http://jcs.biologists.org/cgi/content/full/121/19/3196/DC1

Key words: WASP, Wound, Inflammation, Macrophage, Neutrophil, TILLING

## Introduction

The recruitment of inflammatory cells to sites of tissue damage is one of the most dramatic examples of cell migration in the adult organism, and is absolutely dependent on the capacity of a cell to sense directional cues and to respond to these cues by modifying and re-orientating its actin-rich leading edge to turn towards its target (Pollard and Borisy, 2003). In vitro and in vivo studies indicate that the Rho family of small GTPases are required to transduce these signals to the cytoskeleton (Charest and Firtel, 2007), and that one of these, Cdc42, might control cell polarity via Wiskott-Aldrich syndrome protein (WASp, also known as WASP) family proteins and their regulation of Arp2/3 activity (Ridley et al., 2003). WASp itself is haematopoietically restricted and its close relative, N-WASP, is believed to function in similar ways in other cell lineages. Biochemical and structural studies have defined the functional domains of WASp (Fig. 1A), and indicate it to be folded and autoinhibited in its resting state until bound at its CRIB region by activators, including Cdc42. This leads to unfolding and exposure of its key effector, the VCA domain, which directly binds both Arp2/3 and actin, thus potentially mimicking an actin trimer and serving as a platform for actin polymerisation (Takenawa and Suetsugu, 2007). WASp might be an integral player in leukocyte motility in vivo, as indicated by the human pathology Wiskott-Aldrich syndrome (Ochs and Thrasher, 2006), in which point mutations, generally within exons 1-4 (of 12), in the WIP-binding domain, result in message truncation and failure to translate protein, with the clinical consequence of immunodeficiency characterised by recurrent infections, autoimmunity and bleeding disorders (Jin et al., 2004; Lutskiy et al., 2005). In vitro studies of neutrophils, monocytes and T cells from both patients with Wiskott-Aldrich syndrome and WASp-knockout (KO) mice reveal perturbed migration towards chemotactic cues (Zicha et al., 1998), and, in complementary in vivo studies, leukocytic lineages from WASp-KO mice exhibit a variety of migration and homing defects; for example, a failure of Langerhans cells to emigrate from skin after activation and disrupted dendritic-cell trafficking within T-cell areas (Snapper et al., 2005). However, in these studies, it has not been possible to live image the relevant cell migrations and thus to precisely define how the in vivo immune and/or inflammatory response is disrupted in WASp-deficient cells.

The zebrafish, *Danio rerio*, is emerging as a powerful model organism in which to study disease mechanisms; it is both genetically tractable and, at larval stages, is translucent, making it amenable to live-imaging approaches. Here, we used zebrafish embryos and larvae to image the wound-triggered inflammatory response. We show that knockdown of zebrafish WASps, although not altering total numbers or developmental dispersal of leukocytes

in the organism, dramatically disrupts the wound inflammatory response by perturbing the mechanism by which leukocytes orient towards wound signals. For the first time we are able to dynamically visualise the effects on the in situ inflammatory response of this genetic lesion that is known to dramatically alter inflammatory cell behaviour in human patients.

## Results

### Zebrafish have two WASps, which are both haematopoietically restricted

Within the zebrafish genome, we found four WASp genes (Fig. 1B), consisting of two homologues of *N-WASP* and two genes that are homologous to *WASp* (also known as *wasp1* and *wasp2*), which have 52% and 41% sequence similarity to human WASp, respectively, and 46% similarity to one another (Fig. 1B). The whole-mount in situ expression patterns of zebrafish *wasp1* and *wasp2* in larvae at 3 days post-fertilisation (dpf) appear almost identical, with both genes being expressed both by cells within blood vessels and extravascularly. Those within blood vessels (e.g. Fig. 1G) correspond to thrombocytes and blood-borne leukocytic lineages (monocytes and neutrophils). Outside of vessels, we observed expression by individual cells and groups of cells in locations that correspond to known populations of leukocytes – for example, in regions of the head that correspond to the distribution of macrophages (Herbomel et al., 1999; Herbomel et al., 2001) – and we observed clusters of five or six cells along the flank of the larvae in locations that correspond to those areas in which macrophages are known to associate with the neuromast progenitors of the forming lateral line (Herbomel et al., 2001) (Fig. 1G,H). We performed parallel whole-mount histochemical and immunostaining studies with Sudan Black [which is considered to be a neutrophil-specific marker (Sheehan and Storey, 1947; Le Guyader et al., 2007)] and an antibody against L-plastin [which is pan-leukocyte marker (Le Guyader et al., 2007)], and show that all extravascular WASp1- and WASp2-expressing cells correspond to locations at which macrophages and/or neutrophils reside at these developmental stages (supplementary material Fig. S1). Moreover, quantitative PCR (qPCR) of cells sorted by FACS from a *Tg(lyz:EGFP)* transgenic line in which macrophages and some neutrophils express GFP (Hall et al., 2007) indicates that these leukocytes express both WASp1 and WASp2 at high levels (Fig. 4H).

### Morpholino knockdown of WASp1 disrupts recruitment of primitive macrophages to wounds

To investigate WASp function in vivo, we injected *wasp1*-specific morpholinos into zebrafish embryos at the one-cell stage and compared their wound inflammatory response at 22 hours post-fertilisation (hpf) and 3 dpf with that of sibs injected with control morpholino. To test functionality and WASp-isoform specificity of our morpholino, we co-injected a WASp1-EGFP reporter construct, which is robustly expressed in control-morpholino-injected embryos but entirely knocked down by our *wasp1* morpholino (supplementary material Fig. S2A-B).

At 22 hpf, a stage prior to formation of a primitive circulation, a population of primitive macrophages patrols the yolk sac beneath the epidermis and can be visualised in *Tg(fli1a:EGFP)*-expressing embryos (Lawson and Weinstein, 2002). These cells are rapidly responsive to laser wounds that are made in the epithelial layer (Redd et al., 2006). Embryos in which WASp1 had been knocked down appeared to have normal numbers of primitive macrophages patrolling the yolk prior to wounding, but exhibited a severely reduced wound response. By 1 hour, a mean of only 7.8±0.96 (mean ± s.e.m.; $n$=5) cells had been drawn to the wound, in comparison to 19.6±2.3 ($n$=5) cells in control-morpholino-injected embryos (Fig. 2A-C). These data suggest that the sensitivity or capacity of primitive macrophages to respond to these signals is impaired in WASp1 morphants. In general, migrating cells in control embryos exhibit a clearly polarised morphology with a single leading edge (Fig. 2Di,ii; supplementary material Movie 1), whereas morphant macrophages frequently (in 55% of 27 observed cells) have several leading edges or exhibit a blebbing surface with protrusions extending in all directions (Fig. 2Ei,ii). Moreover, the mean speed of those cells that do respond to the wound cue is also significantly reduced in WASp1-morphant macrophages (5.1±0.29 μm/minute versus 3.6±0.36 μm/minute; $n$=17, five independent experiments, $P=1.7\times10^{-3}$) (Fig. 2C). We also observed differences in the response to contact with other migrating cells: whenever such contacts occurred in control-injected embryos, cells rapidly reoriented and continued on their route towards the wound but, when similar contacts happened in *wasp1*-morpholino-injected embryos, cells withdrew their leading edge and randomly extended protrusions in all directions for some minutes before continuing their migration (supplementary material Movie 2).

### At later larval stages, both neutrophils and macrophages are recruited to tail-fin wounds

Our studies in young embryos, as described above, indicate a function for WASp1 in the basic chemotactic migratory response to wound signals by primitive macrophages at a stage prior to vessel development. At 3 dpf, when a definitive circulation has been established, we investigated how WASps might be required for a more adult-like inflammatory response. We made wounds in the ventral tail fin of 3-dpf larvae, where, prior to wounding, leukocytes are absent (Fig. 3A,B). Scanning electron microscopy (SEM) revealed that the wound epithelium seals very rapidly, so that, by 10 minutes post wounding, epithelial integrity was re-established (Fig. 3C-F). Consistent with previously published results (Mathias et al., 2007; Mathias et al., 2006; Meijer et al., 2008; Renshaw et al., 2006), we observed a robust recruitment of inflammatory cells to such fin wounds. A time-course series of wounds that were stained with Sudan Black, to reveal neutrophils, and an antibody against L-plastin, as a pan-leukocyte marker, revealed that neutrophil numbers peaked at 90 minutes and had generally resolved by 18 hours, whereas L-plastin-positive cells dispersed with a slower time course and, occasionally, cells (presumably macrophages) were still present at 24 hours – at least 6 hours after the last neutrophils had dispersed away from the wound (supplementary material Fig. S3A-C).

Transverse resin sections of the fin wound region indicated the route taken by leukocytes as they migrated from the ventral vein to the site of wound damage (Fig. 3G). Transmission electron microscopy (TEM) enables identification of leukocyte identity by cell morphology, and revealed ultrastructural details of the pathways traversed by these cells (Fig. 3G-M). We observed neutrophils adhering to the endothelial wall in the region of the activated vessel (Fig. 3I), and subsequently migrating through a narrow space filled by matrix and occasional cells, lying between the two epidermal sheets of the tail fin (Fig. 3J). Our TEM studies also gave some indication of the activities of leukocytes once they

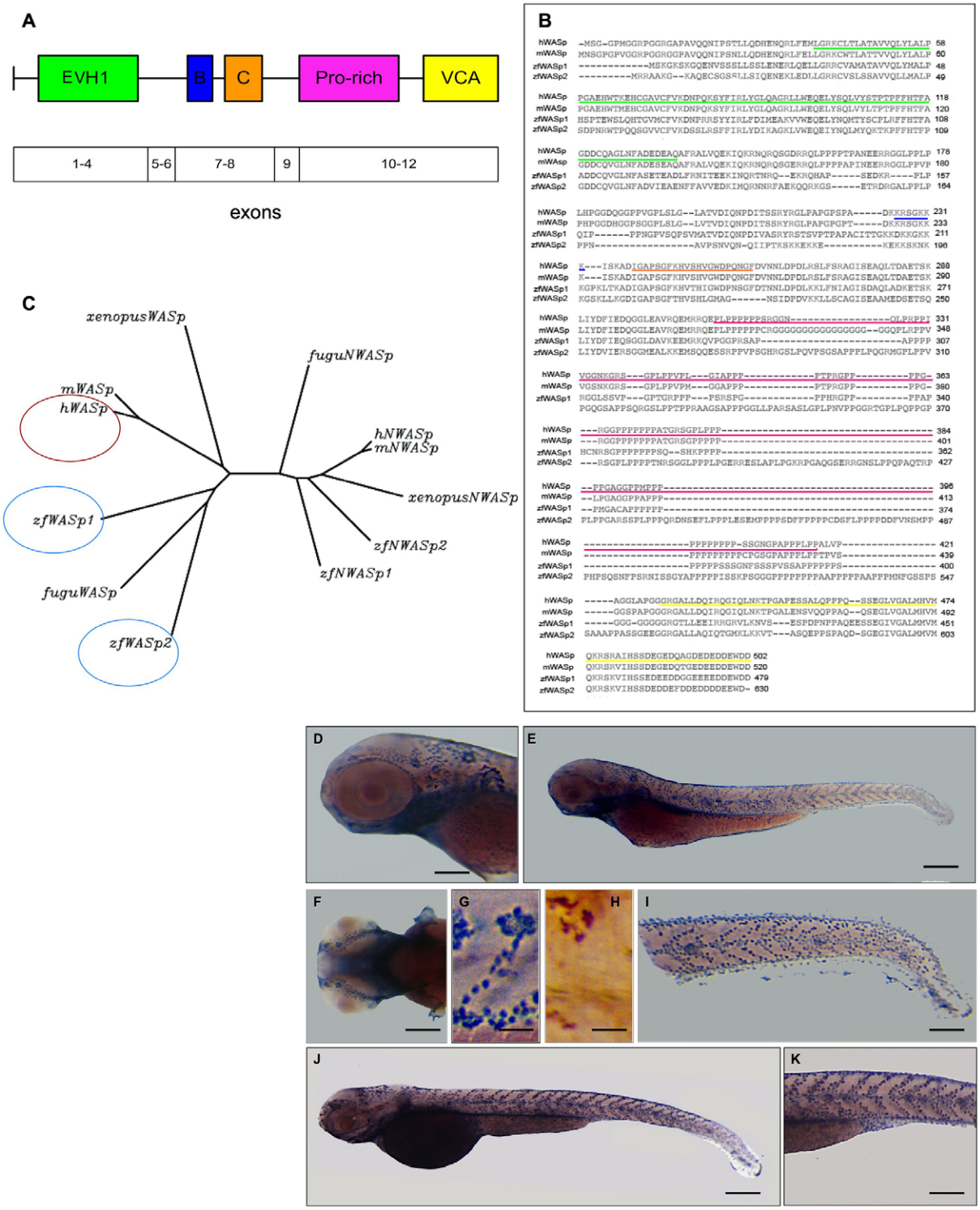


**Fig. 1.** WASp bioinformatics and in situ hybridisation studies. (A) Schematic diagram illustrating the predicted domains in WASp: WASp homology region 1 (EVH1, green), basic (B, blue), minimal high-affinity Cdc42-binding site (C, orange), poly-proline (pro-rich, pink) and VCA (yellow) domains are shown. (B) Alignment of the predicted amino acid sequences of zebrafish (zf prefix) WASp1 and WASp2 with those of human (h prefix) and mouse (m prefix). Multiple alignments were made using the CLUSTALW program as part of the sequence-analysis tools available at the EBI (European Bioinformatics Institute). The underlined sequences represent: green, EVH1 domain; blue, basic domain; orange, minimal high-affinity Cdc42-binding domain site; red, proline-rich domain; yellow, VCA domain. (C) Unrooted dendrogram of the WASp family, including the new zebrafish homologues (circled in blue) of human *WASp* (circled in red). This phylogenetic tree was generated using the GenomeNet Computation Service program. (D-G, I-K) Whole-mount in situ hybridisation expression patterns for WASp1 and WASp2 in 3-dpf zebrafish larvae. WASp1 (D,E,G,I, lateral view; F, dorsal view) and WASp2 (J,K, lateral view) staining indicates expression in haematopoietic cells, leukocytes and thrombocytes (zebrafish platelets). (G) A high-magnification view of an intersomitic vessel indicates WASp-expressing cells both within the vessel and surrounding the adjacent neuromast (lateral-line precursor); staining in the latter corresponds to cells that are also positive for the pan-leukocyte marker L-plastin (H). Scale bars: D, 100 μm; E,J, 250 μm; F, 125 μm; G,H, 20 μm; I, 85 μm; K, 75 μm.

have reached the wound site. Neutrophils are recognisable by their cigar-shaped granules (Fig. 3I-K). Macrophages appear larger and without granules, and most contain evidence of having engulfed cell corpses or matrix debris (Fig. 3L,M). Curiously, in all wounds that we examined, we also saw ultrastructural evidence of junctional links between macrophages and other host cells at the wound site, and we speculate that this might play a role in tethering macrophages in the wound zone (Fig. 3L,M).

### WASp1 and WASp2 morphants exhibit different levels of disruption to the wound inflammatory response

As with early-stage embryos, we saw no sign that the numbers or distribution of leukocytes is altered prior to the wounding of WASp morphants; histochemical studies with Sudan Black and immunostaining with anti-L-plastin antibody indicated no difference from control-treated larvae (supplementary material Fig. S1), and FACS analysis revealed that neither WASp1 nor WASp2 depletion significantly affects the numbers of lysC-expressing leukocytes (Fig. 4I). However, we observed a 42% reduction in the number of Sudan-Black-positive neutrophils recruited to WASp1-morphant versus control wound sites 90 minutes after wounding of the ventral tail fin ($n_{control}$=73, $n_{morphant}$=80, $P$=1.2×10$^{-7}$) (Fig. 4A,B and supplementary material Fig. S3D). We saw an even greater percentage reduction (67%) in the numbers of L-plastin-positive cells at 3 hours post-wounding ($n_{control}$=104, $n_{morphant}$=125, $P$=2.7×10$^{-20}$), suggesting that both neutrophil and macrophage recruitment is perturbed when WASp1 activity is knocked down (Fig. 4D,E and supplementary material Fig. S3E). These data were replicated when we use a second non-overlapping morpholino (supplementary material Fig. S3F,G). Because there are two zebrafish WASps with very similar expression patterns, there is obvious potential for redundancy of function and so we injected one-cell-stage embryos with morpholinos designed to specifically knock down *wasp2*. At concentrations of morpholino that effectively knock down a WASp2-EGFP reporter transgene, but not the WASp1-EGFP reporter (supplementary material Fig. S2A-C′), we saw no significant alteration in the number of Sudan-Black-positive neutrophils recruited to the wound after 90 minutes ($n_{control}$=73, $n_{morphant}$=90, $P$=0.13) compared with control-injected embryos (Fig. 4A,C and supplementary material Fig. S3D). However, WASp2-morphant larvae did exhibit a reduction in the number of L-plastin-positive cells recruited to the wound (although this effect was less severe than for larvae in which WASp1 was knocked down), suggesting that the difference is likely to be due to a defect in macrophage recruitment ($n_{control}$=104, $n_{morphant}$=122, $P$=5.56×10$^{-6}$) (Fig. 4D,F and supplementary material Fig. S3E). When we injected embryos with both *wasp1*- and *wasp2*-specific morpholinos (sufficient to knock down both the WASp1- and WASp2-EGFP reporter), we saw no greater reduction in either neutrophil of macrophage recruitment than if *wasp1* morpholino alone had been injected, suggesting that WASp1 and WASp2 do not act in a synergistic fashion.

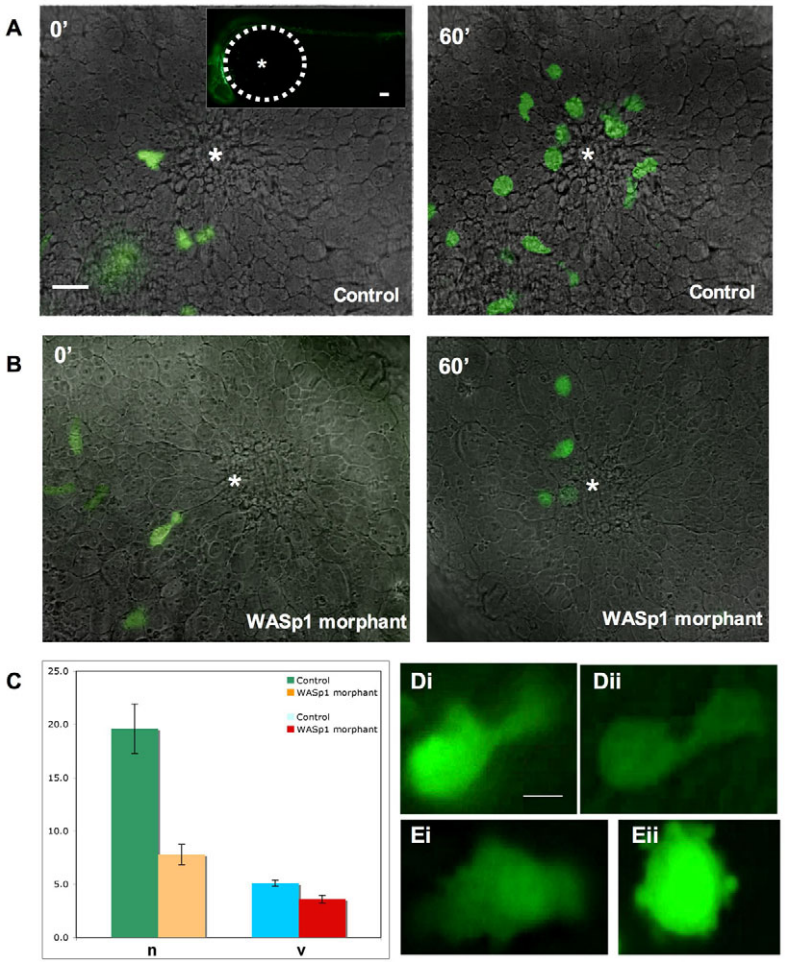


**Fig. 2.** The requirement for WASp1 during the primitive macrophage response to a laser wound. (A,B) Whole-mount views of 22-hpf *Tg(fli1a:EGFP)* transgenic fish with the typical distribution of primitive macrophages (green cells) over the yolk (enclosed by the white broken line in the inset) at 0 minutes (left) and 60 minutes (right) post-wounding of control (A) and WASp1-morphant (B) embryos (wound centre indicated by an asterisk; see supplementary material Movies 1 and 2). (C) A graphic illustration of the number (n, *y*-axis indicates number of cells) of macrophages recruited to control versus morphant wounds and the mean speed (v, *y*-axis indicates mean speed in μm/minute) of these cells. (D,E) Illustrate two typical cell morphologies each of control (D) versus morphant (E) macrophages en route to the wound. Scale bars: A, 20 μm (inset, 50 μm); D,E, 4 μm.

### *Tg(lyz:EGFP)* transgenic fish enable us to fluorescently image leukocyte emigration in WASp1-morphant versus control wounds

To complement our Sudan-Black and L-plastin studies, we also investigated the wound inflammatory response after WASp knockdown using the recently described *Tg(lyz:EGFP)* transgenic fish line, in which a population of macrophages and neutrophils is marked at this stage of development (Hall et al., 2007). Using this fish line to fluorescently live-image the leukocyte response to WASp1 knockdown, we saw no difference in general numbers of GFP-positive cells or in the number of cells associated with the vessel adjacent to the wound, but very few morphant cells commenced migrating towards the wound even by 2 hours (supplementary material Movie 3), by which time there was significant recruitment of GFP-positive cells to control wounds (supplementary material Movie 4). At 3 hours we saw a mean of 8±2.9 (mean ± s.d.; $n$=5) GFP-tagged leukocytes in the vicinity of

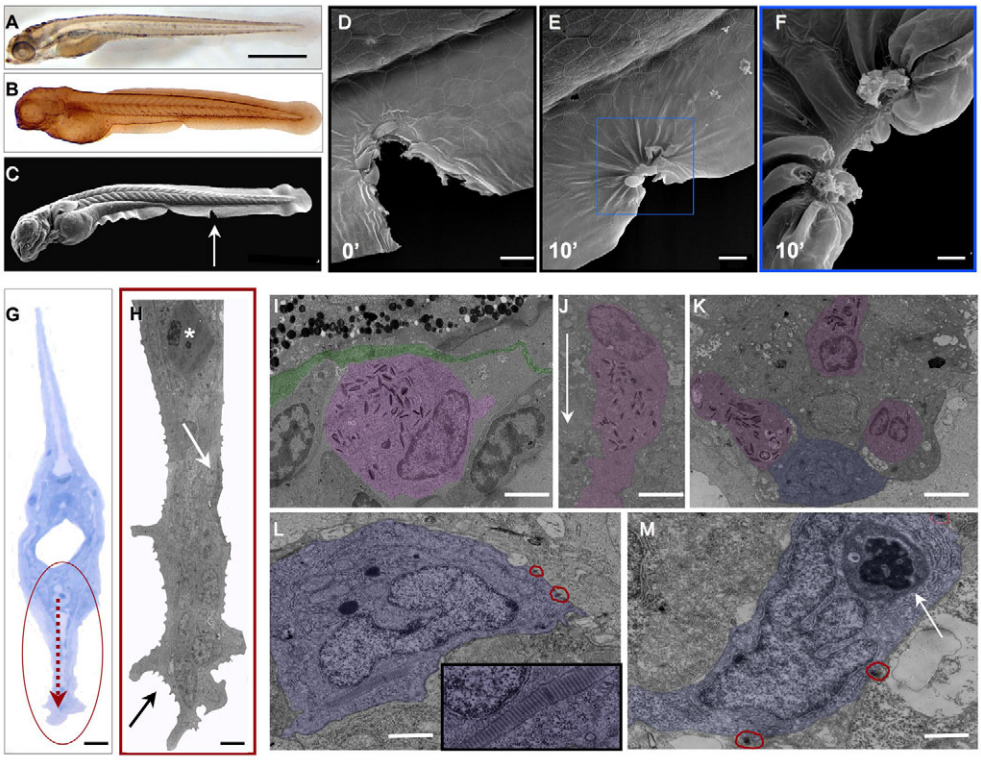


**Fig. 3.** Ultrastructural studies of the fin-wound response. (A,B) Whole-mount 3-dpf larvae prior to wounding that were histochemically stained with Sudan Black to reveal neutrophils (A) or immunostained with L-plastin antibody to reveal macrophages and neutrophils (B), indicating the absence of any leukocytes in the undamaged fin. (C) Scanning electron micrograph (SEM) of a 3-dpf zebrafish larvae fixed immediately post-wounding, indicating the site of lesion (arrow). (D,E) High-magnification views of the wound region at 0 minutes (D) and 10 minutes (E) post-wounding, indicating the rapidity of repair in control larvae. (F) Higher-magnification view of the boxed area in E shows complete epithelial sealing by 10 minutes. (G) Transverse resin section through a Methylene-Blue stained wounded larval tail region; red arrow indicates the route taken by leukocytes from the ventral vein to the site of wound damage in the ventral fin. (H) Transmission electron micrograph (TEM) transverse reconstruction of the entire fin, from the ventral vein (asterisk) to the damaged-fin tip (black arrow). The white arrow indicates fin epithelium. (I-M) False-coloured, high-magnification TEM images corresponding to various steps in the leukocyte migration route from the blood vessel towards the wound. (I) A neutrophil (purple) with characteristic electron-dense cigar-shaped granules is captured as it adheres to the vessel wall (green). (J) Once outside the vessel, the neutrophil changes its morphology, becoming more elongated and polarised as it follows chemotactic cues towards the wound (in the direction of the arrow). (K) Low-magnification TEM illustrating a number of neutrophils and a single macrophage (blue) at the wound site. (L) Illustrates a macrophage that has recently engulfed matrix debris. Areas circled with red indicate desmosomes at junctions between macrophages and adjacent cells at the wound site. The high-magnification inset shows engulfed collagen. (M) Illustrates a macrophage that has engulfed a cell corpse (arrow). Scale bars: A-C, 500 μm; D,E, 20 μm; F, 5 μm. G, 15 μm; H, 5 μm; I,J, 2.5 μm; K, 4 μm; L,M, 2 μm.

control wounds but only 2.3±1.5 (mean ± s.d.; $n$=5) cells had been recruited to morphant wounds (Fig. 4G).

### DIC movies allow us to capture morphologies of all migrating cells and to analyse how WASp knockdown alters leukocyte chemotaxis

Tracking inflammatory cell migrations using transgenic GFP lines, as above, inevitably restricts studies to only those lineages of cells that express the fluorescent tag. Much the same is true for studies using histochemical and/or molecular probes to image specific leukocyte lineages in fixed tissues. To complement these targeted approaches, we made differential interference contrast (DIC) movies, which revealed all those cells that emigrate towards a wound without distinguishing between the various leukocyte lineages.

Our DIC movies indicate that, as cells leave the source vessel, they adopt a polarised morphology with a leading edge consisting of several pseudopodia (Fig. 5E), much like the morphology reported for *Dictyostelium* cells as they migrate up a shallow chemotactic gradient (Andrew and Insall, 2007). These zebrafish leukocytes moved towards the wound at an average speed of approximately 9±0.44 μm/minute (mean ± s.e.m.; $n$=63).

Tracking of leukocyte movements in WASp1-morphant larvae confirmed that fewer cells leave the ventral vein and indicated that those cells that do exhibit a reduced chemotactic index (CI) compared with control larvae (0.55±0.04, $n$=18 versus 0.74±0.02, $n$=50; mean ± s.e.m.; $P=2\times10^{-4}$; Fig. 5C). We observed that the mean cell speed was reduced from 9±0.44 μm/minute ($n$=63) to 5.4±0.51 μm/minute ($n$=35) ($P=2.7\times10^{-7}$), which is in part due to more frequent and longer stopping periods en route (Fig. 5A-D). The morphology of migrating leukocytes in morphant embryos did not appear to be different to that of control larvae: cells still extended several pseudopodia from their leading edge (Fig. 5Fi-iii), but we observed that cells more frequently made the 'wrong' choice of pseudopodia (56%, versus 72% correct turns in control larval cells) and thus fail to turn towards the wound (Fig. 5Fi-iii). Moreover, only in morphant larvae did we see cells stopping en route to the wound and, when this happened, cells exhibited an extremely complex morphology, extending pseudopodia in all

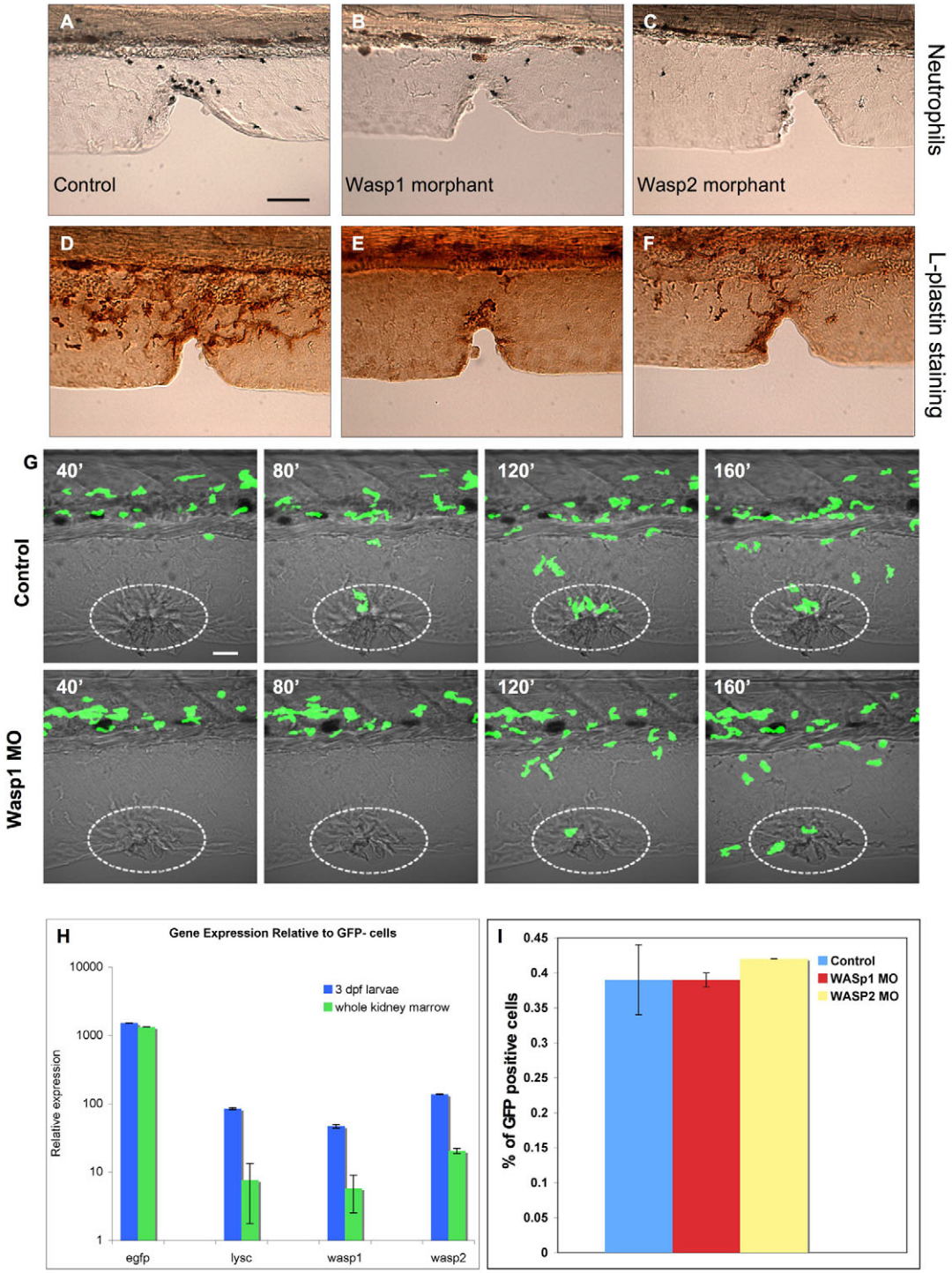


**Fig. 4.** The consequences of *WASp1*- and *WASp2*-morpholino injections on leukocyte recruitment to a fin wound in 3-dpf larvae. (A-C) Typical 90-minute wounds in control- (A), *WASp1*-morpholino-injected (B) and *WASp2*-morpholino-injected (C) larvae after staining with Sudan Black to reveal neutrophil influx to the fin wound. (D-F) Similar wounds, but harvested at 3 hours and immunostained with antibody against L-plastin to reveal the influx of macrophages and neutrophils. (G) Images from a typical fluorescent time-lapse movie of control- and *WASp1*-morpholino-injected (MO) *Tg(lyz:EGFP)* fish after fin wounding; the white dotted ovals indicate wound location. See also supplementary material Movies 3 and 4. (H) qPCR analysis of *egfp*, *lysC*, *wasp1* and *wasp2* expression within EGFP-marked myelomonocytic cells of 3-dpf *Tg(lyz:EGFP)* larvae and *Tg(lyz:EGFP)* whole kidney marrow, relative to that within EGFP-negative cells. Error bars represent standard deviations. (I) FACScan analysis of EGFP-labelled compartments within wild-type, WASp1- and WASp2-depleted 3-dpf larvae. The *y*-axis indicates the percentage of green cells from total cells analysed, and reveals no significant difference between control and WASp-morphant fish. Averages and standard deviations calculated from two separate experiments for each sample are shown. Scale bars: A-F, 25 μm; G, 15 μm.

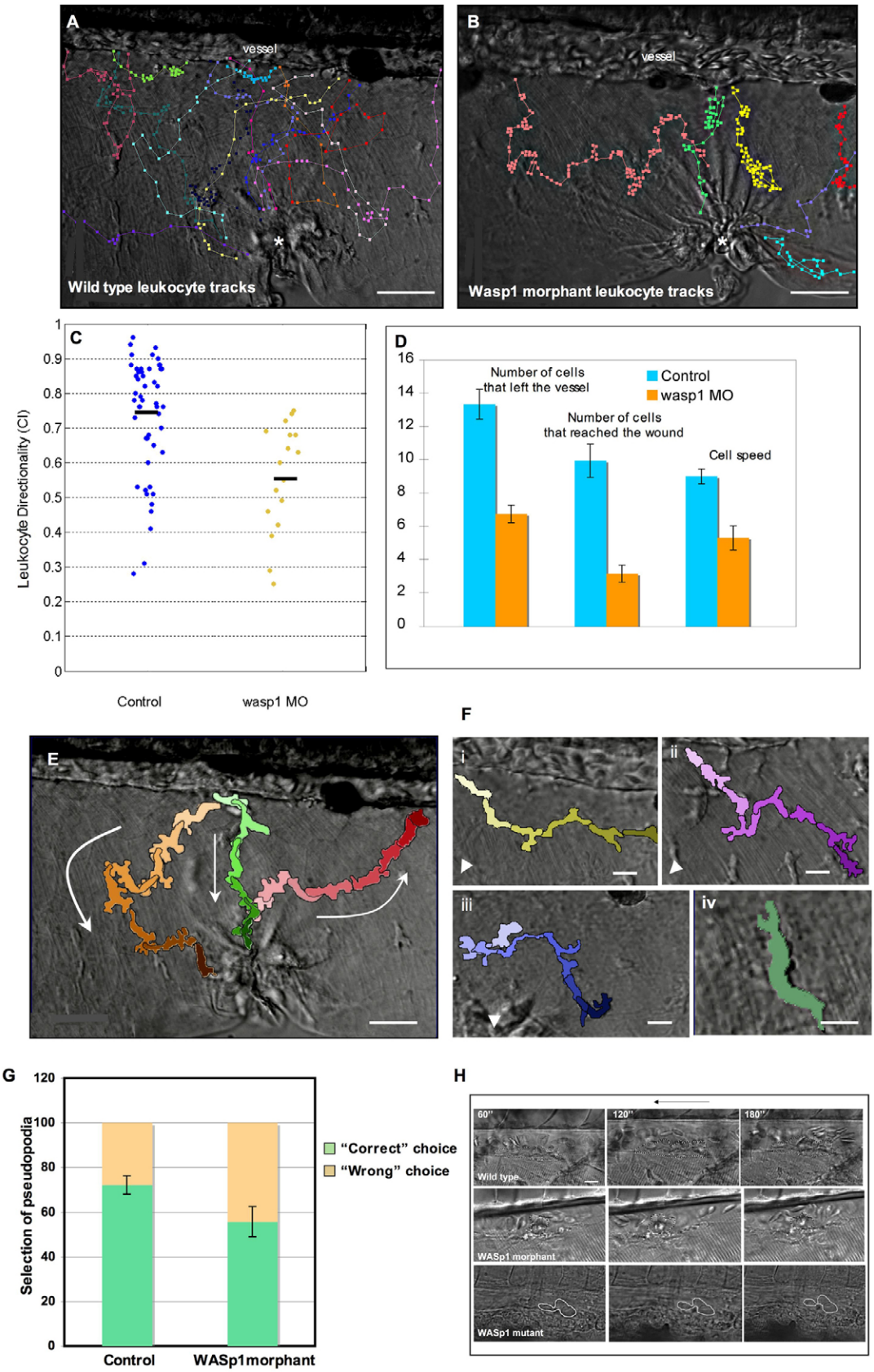


**Fig. 5.** Live-imaging of the wound inflammatory response in WASp-morphant fish and comparison with mutants. (A,B) Cell tracking, from DIC movies, of the inflammatory response at a wound in the ventral tail fin of 3-dpf zebrafish larvae treated with control morpholino (A) or *WASp1* morpholino (B). Cell tracks were generated by marking the centre of the leukocyte every 45 seconds (three frames) from the DIC movie as cells migrated from the vessels to the wound (asterisk). (C,D) Several parameters were analysed: the number of cells that left the vessel up to 3 hours post-wounding (D), the number of cells that successfully navigated to the wound (D), the speed of leukocytes (D, *y*-axis indicates mean speed in μm/minute), and the persistence of their directionality, as indicated by their chemotactic index (CI) (C). (D) Error bars are the standard error of the mean (s.e.m.). (E) Three typical cell tracks, with cell outlines traced at 1- to 2-minute intervals to illustrate cell morphologies during a meandering (orange), a fairly direct (green) or a return (red) journey to and from the wound in a control larvae. (F) False-coloured cell profiles equivalent to those in E, indicating that the morphology of migratory cells (i-iii) does not significantly differ in WASp1-morphant larvae compared with controls, but the pseudopodia choice is frequently 'wrong' and takes the cell away from the wound (wound direction indicated by white arrowhead). When a cell stops, it extends pseudopodia in all directions (see supplementary material Movie 5) and can become elongated (iv). (G) Graphic illustration of the proportion of 'correct' pseudopodia choices made by control versus morphant leukocytes in response to wound signals. (H) DIC micrographs to illustrate the extent of thrombus formation after laser-wounding the aorta at 60, 120 and 180 seconds post-lesion in wild-type, WASp1-morphant and WASp1-mutant fish. Arrow indicates direction of vessel flow. Scale bars: A,B, 30 μm; E, 20 μm; F,H, 10 μm.

directions, occasionally leading to very elongated cells (Fig. 5Fiv and supplementary material Movie 5).

### WASp morphants and mutants exhibit reduced clotting

Because WASp is expressed by thrombocytes and patients with Wiskott-Aldrich syndrome suffer from haemorrhaging defects, we were curious whether the same might be true in zebrafish WASp-morphant larvae. To analyse this, we made microlaser wounds to the aorta and measured the size of the subsequent thrombus. At 3 minutes post-wounding, we found that the thrombus mean size of 1744.96±311.01 μm$^2$ ($n$=5) in wild-type larvae was reduced to 822.11±210.74 μm$^2$ ($n$=6) ($P$=0.02) in WASp1 morphants; this was mirrored in WASp1-mutant (–/– and +/–) fish, in which the mean thrombus size was 575.75±130.09 μm$^2$ ($n$=8; $P$=0.008) (see below and Fig. 5H).

### TILLING for WASp1 mutants produces two mutants that phenocopy our morphant studies and allow longer-term analysis of WASp function

Our morpholino studies of WASp function suggested key roles for WASp1 in the recruitment of leukocytes to wound sites, but the morpholinos were not effective beyond 3 dpf and so we used a TILLING approach (Wienholds et al., 2003) to identify mutants in the *wasp1* gene. We successfully identified two point mutations, one in exon 2 (where the majority of lesions reside in the human syndrome) and the other in exon 10 (within the actin-binding VCA domain) of the gene. To test whether these mutants exhibit a disturbed inflammatory response, we crossed heterozygous parental stocks to generate clutches of larvae in which a quarter were homozygous null individuals. Wounding such clutches, and subsequent genotyping of individual larvae, in parallel with blind

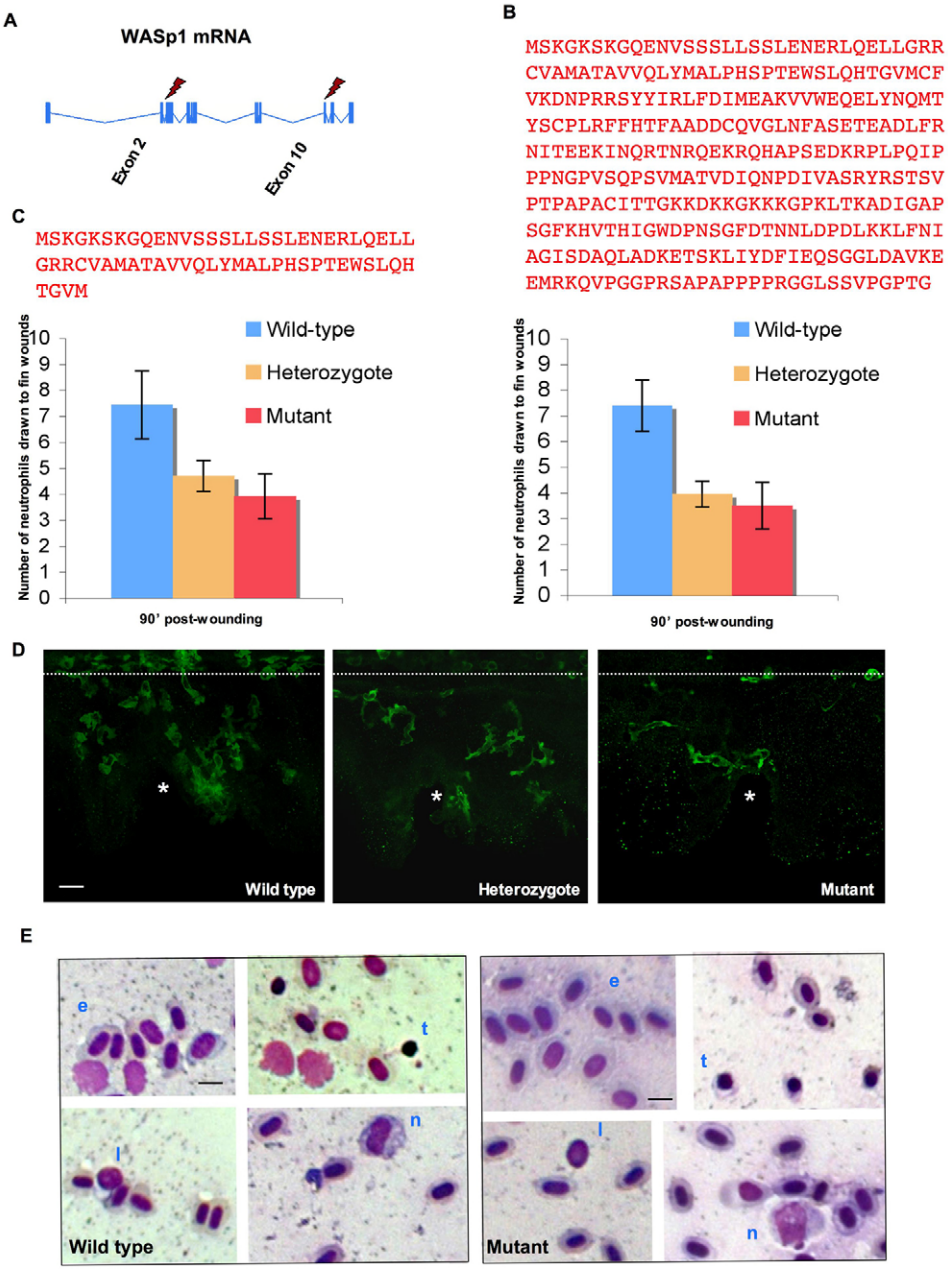


**Fig. 6.** Identification of WASp1 mutants by TILLING. (A) Schematic to illustrate the sites of the two mutations in the *wasp1* gene identified from our TILLING screen. (B,C) Graphic illustrations of the number of neutrophils drawn to 90-minute fin wounds that were made to 3-dpf larvae with the genotypes +/+ (wild type), +/– (heterozygote) and –/– (mutant) derived from +/– × +/– crosses of our exon-2 (B) or exon-10 (C)-mutant lines. Amino acids remaining post stop codon are highlighted in red. (D) Illustrates fluorescent immunostaining of typical wild-type, heterozygote and WASp1-mutant wounds at 3 hours post-wounding to indicate the differential extent of leukocyte recruitment; the broken white line indicates the ventral margin of the vein and the asterisk marks the centre of the wound. (E) Blood smears from 1-month-old WASp1-mutant (exon 10) fish versus control sibs to illustrate morphologies of erythrocytes (e), thrombocytes (t), neutrophils (n) and lymphocytes (l). Scale bars: D, 15 μm; E, 4 μm.

Sudan-Black histochemical staining to reveal neutrophil numbers, indicated that WASp1 mutant larvae are, as are morphants, defective in their capacity to recruit neutrophils to a wound, with numbers reduced to 47% of wild-type levels in the exon-2 mutant ($n$=79, $P$=1.7×10$^{-2}$) and 53% in the exon-10 mutant ($n$=77, $P$=6.6×10$^{-3}$) (Fig. 6B,C). For both of these lines, the heterozygous larvae also exhibited a similar reduction in wound neutrophil numbers to those seen in the mutants. Immunostaining with anti-L-plastin antibody (which reveals both neutrophils and macrophages) showed a clear reduction in the number of leukocytes that were recruited to mutant wounds, with a mean of 3.5 cells, versus 9.23 cells in an equivalent 3-hour wild-type wound ($n$=50, $P$=0.02) (Fig. 6D).

At least until 30 dpf, homozygous mutant fish (exon 10) remained viable and blood smears indicated no obvious morphological defects in white blood cells or thrombocytes when compared with their wild-type sibs (Fig. 6E).

## Discussion

One major advantage of performing these studies in zebrafish embryos and larvae is their translucency, which, for the first time, has allowed us to make direct in vivo observations of WASp-deficient leukocytes as they attempt to respond to tissue-damage cue(s). Both primitive macrophages and, after a definitive circulation has been established, neutrophils and macrophages exhibit impaired average migratory speed and directionality towards wounds. At the later stage, of the two zebrafish WASps, WASp1 appears to have a non-redundant and significant role in both neutrophil and macrophage emigration, whereas WASp2 plays a less significant role and we only saw reduced efficiency of macrophage migration to wounds. This difference between the two WASps is unlikely to be because of different spatial regulation, because they appear to be expressed almost identically. Neither is it likely to be due to expression levels, because our in situ data and qPCR data both indicate that, if anything, there is more *wasp2* mRNA than *wasp1* mRNA expressed by leukocytes.

Our studies offer new insight into what role WASps might be playing in the navigation of leukocytes towards chemotactic cues. Clearly, at early embryonic stages the normal polarised morphology of migrating primary macrophages is altered, as previously described for *WASp*-null macrophages in vitro (Calle et al., 2004) and this might contribute to their poor capacity to navigate towards the wound. However, with the later-stage leukocytes, which, in vivo, migrate more as a *Dictyostelium* amoeba by selective choice of pseudopodia (Andrew and Insall, 2007), it appears that migratory morphology remains unchanged in WASp1-morphant cells, but the capacity to choose the 'correct' pseudopodia is severely disrupted. Hence, the WASp1-morphant cells make more wrong turns and so chemotaxis is significantly less efficient.

For both the primitive macrophages and later-stage leukocytes, the failure of WASp-deficient cells to navigate accurately is more exaggerated when the cell has stopped and has to start again; for example, when two primitive macrophages collide and take an aberrantly long time to reorient, or a leukocyte stops and then appears to protrude pseudopodia in all directions. These observations suggest that the breaking of symmetry to reinstate directed cell migration is particularly sensitive to loss of WASp activity.

What is very clear from both our morphant and mutant data is that, although the migration of leukocytes towards wound cues is severely disrupted in WASp-deficient cells, the numbers and developmental dispersal of all the lineages we examined appears close to normal and, at 3 dpf, both the numbers of these cells and their locations within the embryo are no different from that of wild-type control larvae. Although intuitively it might seem likely that similar cues would be used to guide leukocytes to their correct developmental locations and subsequently to sites of tissue damage, there is already a precedent in the *Drosophila* embryo indicating that the signals guiding developmental and wound migrations of macrophages might be dramatically different, with one being PI3K dependent and the other not (Wood et al., 2006).

By TILLING for mutations in the early exons of *wasp*, where there are hotspots for the genetic lesions in human patients, as well as those closer to the VCA effector domain, we expected to model the effects in vivo of a true null versus a dominant-negative allele, and yet our heterozygote larvae from both mutant crosses exhibited a phenotype close to that of homozygous mutant individuals. This might be because both our mutants are functioning as dominant-negative proteins by mopping up activator signals, but there might also be a threshold effect that will require further study. Whereas heterozygous larvae exhibited a retarded wound inflammatory response, they were viable and fertile, and might provide opportunities for future studies of autoimmune-related aspects of the Wiskott-Aldrich syndrome. Both morphants and mutants exhibited a thrombosis and/or bleeding phenotype that mirrored the human syndrome, although thrombocytes appeared not to have a different morphology to those in control fish. Clearly, zebrafish thrombocytes are very different from megakaryocyte-derived platelets in mice and man, but because it is clear that the defect in platelets from Wiskott-Aldrich patients is not simply in their capacity to assemble actin or change shape (Falet et al., 2002), our fish model might also offer some opportunities to understand the mechanisms underlying defective clotting.

Recently, zebrafish have come to the fore as a model in which to investigate human disease, and they are particularly suited to diseases that involve disruption of the immune response because they are very genetically tractable and their translucency makes them ideal for live-imaging of the cell migrations that underlie most immune responses. At both early-embryonic and larval stages, zebrafish have also proven to be very amenable to drug manipulations of the immune response (Brown et al., 2007; Redd et al., 2006). In this study, we report the first analysis of a model of a human inflammatory cell syndrome in zebrafish, and our studies confirm and add to what has previously been gleaned from in vitro studies of mammalian cells that are deficient in WASp and in vivo studies in mouse and man, in which it has not been possible to live-image the cell-migration defects as we can in fish. Presumably, similar studies will be possible for other immune and/or inflammatory diseases, and will be greatly aided by the transgenic lines now available that fluorescently tag the various immune-cell lineages. Such studies will enable a broad analysis of gene function during various inflammatory processes, in ways that will be of great value when discovering the key signalling pathways that underlie the various vertebrate immune responses and which of these might be most therapeutically tractable.

## Materials and Methods

### Characterisation of the WASps in zebrafish

The zebrafish genomic database (http://www.ensembl.org/Danio_rerio/index.html) was searched for *WASp* homologues, and protein-family relationships were analysed using the PROSITE database (http://www.expasy.org/prosite/). Two potential *WASp* homologues were identified: Ensembl transcript ID ENSDART00000039080 (referred to as *wasp1*) and Ensembl transcript ID ENSDART00000026807 (*wasp2*). These were used to determine the full-length sequence for the two zebrafish WASps (Fig.

1B). Multiple sequence alignments were made using the CLUSTALW program as part of the sequence analysis tools available at the European Bioinformatics Institute (EBI) and an unrooted phylogenetic tree was generated from this alignment (Fig. 1C).

### Whole-mount in situ hybridisation

Larvae were processed for whole-mount in situ hybridisation as previously described (Thisse et al., 1993). In brief, antisense-mRNA digoxigenin (DIG)-labelled probes were generated using a *wasp1* construct, GenBank accession no. BC053291 and the first 391 bp of *wasp2* cDNA derived from wasp2pCR4-TOPO construct. After overnight hybridisation with probe at 56°C and buffer rinses, larvae were incubated for 2 hours at room temperature (RT) in anti-digoxigenin antibody before washing and colour developing for 24 hours using nitro blue tetrazolium chloride (NBT)/BCIP (5-bromo-4-chloro-3-indolyl phosphate toluidine salt) as substrate. Photomicrographs were taken with a Leica camera (DFC320) attached to a Leica MZFLIII dissecting microscope.

### Sudan-Black staining of neutrophils

In order to identify neutrophils in control- and morpholino-treated 3-dpf zebrafish embryos, Sudan-Black staining was performed as described previously (Sheehan and Storey, 1947). Embryos were fixed 90 minutes after wounding in 4% glutaraldehyde in buffer for 30 minutes at RT and then stained with 0.18% Sudan Black, followed by extensive washing in 70% ethanol.

### Transmission and scanning electron microscopy

3-dpf larvae were fixed in a mixture of 2% paraformaldehyde and 2% glutaraldehyde in 0.1 M cacodylate buffer (pH 7.4) over night, and postfixed in 1% osmium tetroxide for 1 hour. The embryos were then rinsed in buffer, dehydrated in a graded ethanol series and those for TEM were embedded in Epon. These embryos were oriented for transverse sections and serial thick sections (1 μm) were stained with Methylene Blue for light-microscopic analysis. Thin sections (around 60 nm) were stained with uranyl acetate and lead citrate, then viewed by TEM (Philips CM100). Embryos for SEM were critically point dried in $CO_2$ immediately post dehydration, before being mounted on stubs, sputter coated with gold and viewed by SEM (Philipps 501B).

### *wasp1* and *wasp2* antisense-oligo injections

Morpholinos targeting zebrafish *wasp1* (5′-GCCCTTTGCTTTTGCCTTTGCTCAT-3′ and 5′-ATAGCCTGCGCACAAACACATTAAA-3′), *wasp2* (5′-CTTTCCCC TTCGCGGCTCGCCTCAT-3′ and 5′-CAGAGACTGCAGACAA AAACACAAA-3′) and standard control oligo (5′-CCTCTTACCTCAGTTACAATTTATA-3′) were obtained from GeneTools LLC. The oligos were resuspended in sterile water and approximately 1 nl was injected into zebrafish embryos, at the one- to two-cell stage, at a range of 1-4 μg/μl until an optimal concentration was identified. Antisense oligos were injected either alone or in combination. For *wasp1,* a concentration of 1-1.5 μg/μl was used in further experiments and 2 μg/μl for *wasp2*. The standard control oligo was injected at 2 μg/μl.

### Wounding and DIC video microscopy

3-dpf larvae were transferred into a dish containing 2-4% anaesthetic (MS-222) in 30% Danieu's solution, to prevent embryos from twitching. Embryos were embedded laterally in a small drop of 1.2% low-melting agarose, in a 100 mm Petri dish, for wounding of the fin and subsequent time-lapse imaging. Consistent wounds were made with sharpened tungsten needle to the middle of the ventral tail fin. Time-lapse imaging was performed using DIC microscopy on a Zeiss Axioplan 2 and 40× oil objective. Images were taken every 15 seconds for up to 3 hours using Improvision OpenLab software (see below).

### Cell tracking of leukocyte recruitment to the wound

We used Improvision Volocity 3.1 software to analyse leukocyte recruitment to the larval tail-fin wound, with each cell tracked from when it left the vessel until it reached the wound. Cell tracks were generated from the DIC movie by marking the centre of the leukocyte every 45 seconds (three frames). From five control and five morphant larvae we analysed the number of cells that left the vessel up to 3 hours post-wounding, the number that successfully navigated to the wound, the speed of leukocytes and their directional persistence, as indicated by their CI. Average speed was calculated for each cell by dividing the distance travelled by the time taken to reach the wound. CI was defined as the ratio between the shortest linear distance (from start to end point) and the total distance travelled by the cell. CI was calculated only for cells that reached the wounds at any point of their 'journey' and a higher CI indicates a more directed and/or persistent pathway of migration. The morphology of cells at various time points during their migratory route was captured from individual frames of time-lapse movies using Adobe ImageReady CS2 and tracing cell profiles, which we subsequently false coloured (darker shades to indicate progressing time). These profiles outlined the leading-edge pseudopodia and enabled us to determine whether a cell had made a 'correct' or 'wrong' choice of pseudopodia at each of its turning points en route to the wound, i.e. a 'correct' choice of two pseudopodia is that pseudopodia with the smallest angle away from a line linking the centroid of the cell to the wound centre. This analysis was performed on five morphant and 14 control cells with a range of 10-15 turns per cell.

### Yolk-sac laser wounding and generating thrombi

Five control and five morphant 22-hpf *Tg(fli1a:EGFP)* embryos were dechorionated and mounted laterally on a glass slide in a small drop of 1.2% low-melting agarose loaded with 0.003% tricaine. Embryos were wounded on the epidermal surface overlying the yolk using a UV-nitrogen laser microbeam coupled to a Zeiss Axioplan 2 microscope and 40× oil objective (Micropoint Laser System, Photonic Instruments) (Redd et al., 2006). Each laser wound was approximately 50 μm in diameter. Epi-fluorescent images were taken every 15 seconds for up to 1 hour using OpenLab software. We used the same laser to trigger formation of thrombi in 3-dpf larvae by wounding the endothelium of the aorta. The size of the resulting thrombus was measured as an area from DIC images at 3 minutes post-wounding. At least six larvae were used for each of the control, morphant and mutant vessel lesions.

### Imaging inflammation in *Tg(lyz:EGFP)* transgenic animals

Wounds were made to the ventral fin (as above) of anaesthetised 3-dpf *Tg(lyz:EGFP)* transgenic larvae prior to embedding in agar. Time-lapse confocal microscopy was performed using an Olympus FV1000 confocal microscope equipped with a heated chamber maintained at 29°C. *z*-series were collected at 1.5-minute intervals. Projections of summed *z* stacks, time-lapse animations and cell tracking were generated using ImageJ (Abramoff et al., 2004).

### FACS and qPCR analysis

Larval dissociation was carried out as previously described (Covassin et al., 2006) with modifications, for about 200 each of 3-dpf *Tg(lyz:EGFP)* larvae that had previously been injected with 1 ng of either the *wasp1*- or *wasp2*-targeting morpholinos. In brief, larvae were dechorionated by pronase treatment and de-yolked in calcium-free Ringer solution by passage through a 200 μl pipette tip. Cells were disaggregated by further agitation in 0.25% trypsin-EDTA for 1.5 hours at 28.5°C and disaggregated cells were centrifuged for 3 minutes at 3000 rpm before resuspension in 0.9× PBS (pH 7.4), 5% FCS. Cells were then passed several times through 40-μm cell strainers (BD Falcon) to remove debris. Whole kidney marrow preparations were generated as previously described (Traver et al., 2003). FACS analysis was based on forward and side scatter characteristics, propidium-iodide exclusion and GFP fluorescence using a FACS Vantage flow cytometer (Becton Dickinson). Cells were sorted directly into ice-cold cell-lysis buffer (Cells-to-cDNA II kit, Ambion) and cDNA generated. Real-time PCR was performed using Platinum SYBR Green qPCR SuperMix (Invitrogen). Quadruplicate samples were analysed by relative quantitation with EGFP-negative cells as calibrator. Error bars represent standard deviation. Oligonucleotide sequences were as follows: ef1α forward, 5′-TGCCTTCGTCCCAATTTCAG-3′; ef1α reverse, 5′-TACCCTCCTTGCGCT-CAATC-3′; egfp forward, 5′-GAGCTGAAGGGCATCGACTT-3′; egfp reverse, 5′-TGCTTGTCGGCCATGATATAGA-3′; lysC forward, 5′-GTGAAAATG-GACGGGCTGAA-3′; lysC reverse, 5′-CTTTGTTTGCGCTGCTCACA-3′; wasp1 forward, 5′-AGTGGATTCAAACACGTCACTCA-3′; wasp1 reverse, 5′-CCAGCA-ATGTTGAACAGTTTCTTC-3′; wasp2 forward, 5′-AATGAGAAGCTG-GAGGATCTG-3′; wasp2 reverse, 5′-TTGTGGTGTCCATCGATTCG-3′.

All oligonucleotides were designed to span introns as a control for genomic contamination.

### TILLING for WASp1 mutants

Two mutations in *wasp1* (gene ID: ENSDARG00000026350) were identified in exon ENSDARE00000239556 (hu3280) and exon ENSDARE00000239483 (hu3279) using target-selected mutagenesis (TILLING) of ENU-mutagenised parental stock as previously described (Stemple, 2004; Wienholds et al., 2003). Heterozygote fish from each line were crossed and we made wounds in the ventral fins of their 3-dpf offspring as described above. Prior to fixation, embryos were decapitated and heads were used for genotyping. Primers for this genotyping were as follows: Wasp-10-1, 5′-GCACAATAATATGTCCCAGTG-3′; Wasp-10-2, 5′-TGTAAAACGACGGCCA-GTTTTCATCGTGCCCTTTG-3′; Wasp-10-3, 5′-AGGAAACAGCTATGAC-CATGGCTACTGGAGAAGTTACCG-3′; Wasp-10-4, 5′-TTCCTCCAGTAA-AGTTCCTCTC-3′; Wasp-2-1, 5′-AACTGGAGAGAGACGACAGG-3′; Wasp-2-2, 5′-TGTAAAACGACGGCCAGTGATGCTGATTTCTGTGCTTG-3′; Wasp-2-3, 5′-AGGAAACAGCTATGACCATTCTCTGTCTGCATACGTTCTG-3′; Wasp-2-4, 5′-TCAGTTTACCATCTCATTGGAC-3′.

### Blood smears from WASp1 mutants

To identify any potential morphological differences between wild-type and WASp1-mutant white blood cells and thrombocytes, we collected blood from the tail vein of 1-month-old larvae and stained smears with May Grunwald-Giemsa stain (Lieschke et al., 2001). Photomicrographs of blood smears were taken with an AxioCam HR camera attached to a Zeiss Axio Imager M1 microscope.

This work was supported by the Wellcome Trust; by an ORS and University of Bristol Scholarship to A.C.; and by a NERF grant from

the Foundation for Research Science and Technology, New Zealand. We are indebted to Debbie Carter, Bob Porter and David Woolley for their invaluable guidance and practical assistance with our scanning and transmission electron microscopy studies. We thank Edwin Cuppen and Roland Plasterk (Hubrecht Laboratory) and Derek Stemple (Wellcome Trust Sanger Institute) for providing the zebrafish knockout mutant, which was generated as part of the ZF-MODELS Integrated Project in the 6th Framework Programme (contract no. LSHG-CT-2003-503496), funded by the European Commission. Thanks also to Derek Stemple, Ross Kettleborough, Colin Herd, Elizabeth Busch-Nentwich and Kerstin Jekosch for constant bioinformatics and fish support on our many trips to the Sanger. Finally, thanks to Jonathan Clarke, Giles Cory, Gareth Jones, Catherine Nobes and Yi Feng for ongoing WASp and cell-migration advice, and comments on the manuscript.

## References

**Abramoff, M., Magelhaes, P. and Ram, S.** (2004). Image Processing with ImageJ. *Biophotonics Int.* **11**, 36-42.

**Andrew, N. and Insall, R. H.** (2007). Chemotaxis in shallow gradients is mediated independently of PtdIns 3-kinase by biased choices between random protrusions. *Nat. Cell Biol.* **9**, 193-204.

**Brown, S. B., Tucker, C. S., Ford, C., Lee, Y., Dunbar, D. R. and Mullins, J. J.** (2007). Class III antiarrhythmic methanesulfonanilides inhibit leukocyte recruitment in zebrafish. *J. Leukoc. Biol.* **82**, 79-84.

**Calle, Y., Chou, H. C., Thrasher, A. J. and Jones, G. E.** (2004). Wiskott-Aldrich syndrome protein and the cytoskeletal dynamics of dendritic cells. *J. Pathol.* **204**, 460-469.

**Charest, P. G. and Firtel, R. A.** (2007). Big roles for small GTPases in the control of directed cell movement. *Biochem. J.* **401**, 377-390.

**Covassin, L., Amigo, J. D., Suzuki, K., Teplyuk, V., Straubhaar, J. and Lawson N. D.** (2006). Global analysis of hematopoietic and vascular endothelial gene expression by tissue specific microarray profiling in zebrafish. *Dev. Biol.* **299,** 551-562.

**Falet, H., Hoffmeister, K. M., Neujahr, R. and Hartwig, J. H.** (2002). Normal Arp2/3 complex activation in platelets lacking WASp. *Blood* **100**, 2113-2122.

**Hall, C., Flores, M., Storm, T., Crosier, K. and Crosier, P.** (2007). The zebrafish *lysozyme C* promoter drives myeloid-specific expression in transgenic fish. *BMC Dev. Biol.* **7**, 42.

**Herbomel, P., Thisse, B. and Thisse, C.** (1999). Ontogeny and behaviour of early macrophages in the zebrafish embryo. *Development* **126**, 3735-3745.

**Herbomel, P., Thisse, B. and Thisse, C.** (2001). Zebrafish early macrophages colonize cephalic mesenchyme and developing brain, retina, and epidermis through a M-CSF receptor-dependent invasive process. *Dev. Biol.* **238**, 274-288.

**Jin, Y., Mazza, C., Christie, J. R., Giliani, S., Fiorini, M., Mella, P., Gandellini, F., Stewart, D. M., Zhu, Q., Nelson, D. L. et al.** (2004). Mutations of the Wiskott-Aldrich Syndrome Protein (WASP): hotspots, effect on transcription, and translation and phenotype/genotype correlation. *Blood* **104**, 4010-4019.

**Lawson, N. D. and Weinstein, B. M.** (2002). In vivo imaging of embryonic vascular development using transgenic zebrafish. *Dev. Biol.* **248**, 307-318.

**Le Guyader, D., Redd, M. J., Colucci-Guyon, E., Murayama, E., Kissa, K., Briolat, V., Mordelet, E., Zapata, A., Shinomiya, H. and Herbomel, P.** (2007). Origins and unconventional behavior of neutrophils in developing zebrafish. *Blood* **111**, 132-141.

**Lieschke, G. J., Oates, A. C., Crowhurst, M. O., Ward, A. C. and Layton, J. E.** (2001). Morphologic and functional characterization of granulocytes and macrophages in embryonic and adult zebrafish. *Blood* **98**, 3087-3096.

**Lutskiy, M. I., Rosen, F. S. and Remold-O'Donnell, E.** (2005). Genotype-proteotype linkage in the Wiskott-AlPDFLabdrich syndrome. *J. Immunol.* **175**, 1329-1336.

**Mathias, J. R., Perrin, B. J., Liu, T.-X., Kanki, J., Look, A. T. and Huttenlocher, A.** (2006). Resolution of inflammation by retrograde chemotaxis of neutrophils in transgenic zebrafish. *J. Leukoc. Biol.* **80**, 1281-1288.

**Mathias, J. R., Dodd, M. E., Walters, K. B., Rhodes, J., Kanki, J. P., Look, A. T. and Huttenlocher, A.** (2007). Live imaging of chronic inflammation caused by mutation of zebrafish Hai1. *J. Cell Sci.* **120**, 3372-3383.

**Meijer, A. H., van der Sar, A. M., Cunha, C., Lamers, G. E. M., Laplante, M. A., Kikuta, H., Bitter, W. and Becker, T. S. a. S. H. P.** (2008). Identification and real-time imaging of a myc-expressing neutrophil population involved in inflammation and mycobacterial granuloma formation in zebrafish. *Dev. Comp. Immunol.* **32**, 36-49.

**Ochs, H. D. and Thrasher, A. J.** (2006). The Wiskott-Aldrich syndrome. *J. Allergy Clin. Immunol.* **117**, 725-738; quiz 739.

**Pollard, T. D. and Borisy, G. G.** (2003). Cellular motility driven by assembly and disassembly of actin filaments. *Cell* **112**, 453-465.

**Redd, M., Kelly, G., Dunn, G., Way, M. and Martin, P.** (2006). Imaging macrophage chemotaxis in vivo: Studies of microtubule function in zebrafish wound inflammation. *Cell Motil. Cytoskeleton* **63**, 415-422.

**Renshaw, S. A., Loynes, C. A., Trushell, D. M. I., Elworthy, S., Ingham, P. W. and Whyte, M. K. B.** (2006). A transgenic zebrafish model of neutrophilic inflammation. *Blood* **108**, 3976-3978.

**Ridley, A. J., Schwartz, M. A., Burridge, K., Firtel, R. A., Ginsberg, M. H., Borisy, G., Parsons, J. T. and Horwitz, A. R.** (2003). Cell migration: integrating signals from front to back. *Science* **302**, 1704-1709.

**Sheehan, H. and Storey, G.** (1947). An improved method of staining leukocyte granules with Sudan Black B. *J. Pathol. Bacteriol.* **59**, 336.

**Snapper, S. B., Meelu, P., Nguyen, D., Stockton, B. M., Bozza, P., Alt, F. W., Rosen, F. S., von Andrian, U. H. and Klein, C.** (2005). WASP deficiency leads to global defects of directed leukocyte migration in vitro and in vivo. *J. Leukoc. Biol.* **77**, 993-998.

**Stemple, D. L.** (2004). TILLING – a high-throughput harvest for functional genomics. *Nat. Rev. Genet.* **5**, 145-150.

**Takenawa, T. and Suetsugu, S.** (2007). The WASP-WAVE protein network: connecting the membrane to the cytoskeleton. *Nat. Rev. Mol. Cell. Biol.* **8**, 37-48.

**Thisse, C., Thisse, B., Schilling, T. F. and Postlethwait, J. H.** (1993). Structure of the zebrafish snail1 gene and its expression in wild-type, spadetail and no tail mutant embryos. *Development*. **119**, 1203-1215.

**Traver, D., Paw, B. H., Poss, K. D., Penberthy, W. T, Lin, S. and Zon, L. I.** (2003). Transplantation and in vivo imaging of multilineage engraftment in zebrafish bloodless mutants. *Nat. Immunol.* **4**, 1238-1246.

**Wienholds, E., van Eeden, F., Kosters, M., Mudde, J., Plasterk, R. H. A. and Cuppen, E.** (2003). Efficient target-selected mutagenesis in zebrafish. *Genome Res.* **13**, 2700-2707.

**Wood, W., Faria, C. and Jacinto, A.** (2006). Distinct mechanisms regulate hemocyte chemotaxis during development and wound healing in Drosophila melanogaster. *J. Cell Biol.* **173**, 405-416.

**Zicha, D., Allen, W. E., Brickell, P. M., Kinnon, C., Dunn, G. A., Jones, G. E. and Thrasher, A. J.** (1998). Chemotaxis of macrophages is abolished in the Wiskott-Aldrich syndrome. *Br. J. Haematol.* **101**, 659-665.